Orbital Angular Momentum Generation in a 60-GHz Wireless Radio Channel

Fariborz Eslampanahi Mahmouli, *Member, IEEE,* and Stuart Walker

***Abstract* — We describe transmission of 4-Gbps uncompressed video utilizing a 60-GHz wireless channel with orbital angular momentum (OAM). The laboratory experiments were supported by Matlab simulation; this being utilized to generate holographic masks. Matlab code was further employed to control a printed circuit board (PCB) router drill. Any required shape on, for instance, copper or dielectric plates could be produces. An experimental setup was arranged to validate the transmission performance of 4-Gbps uncompressed video over 60-GHz OAM wireless channel we believe, for the first time. Good agreement was achieved between simulated and measured results. It is concluded that it is practically feasible to send multi-gigabit wireless data over an OAM channel.**

***Keywords* — Antenna arrays, channel capacity, millimeter wave propagation, orbital angular momentum, wireless communication.**

I. Introduction

THE 60-GHz wireless frequency band includes 7 GHz of unlicensed bandwidth [1-3]. This is useful for multi-gigabit data rate applications in wireless communications such as high definition video content and large data files. The uses of wireless communication devices in consumer electronics are expanding fast. In particular, multi-gigabit video and data file transfers require a fast and effective wireless communication method [4]. Thus, very good opportunities are available since the release of the 60-GHz band. Attenuation due to oxygen absorption at 60-GHz is approximately 1.5 dB per 100 m [2, 5, 6] which can be beneficial for operating multiple wireless communication links in the same environment as a high degree of spectrum reuse is available.

From Maxwell's theory, both energy and momentum are carried by electromagnetic radiation. The momentum is comprised of linear and angular contributions. With angular momentum, polarization is associated with spin part and spatial distribution is associated with the orbital part. In this research, two distinct methods of creating orbital angular momentum (OAM) in the radio domain are examined by simulation and experimental procedures. Many authors e.g. [7-14] have investigated the OAM states of optical and wireless signals. However, to our knowledge, a 60-GHz OAM channel has not been utilized to transmit 4-Gbps uncompressed video. In order to demonstrate the practicality of the technique, an OFDM 60-GHz millimeter wavelength reference system produced by *Silicon Image* [15] was utilized. Simulation models were compared to the measured results by placing a spiral phase plate (SPP) or holographic plate (HP) directly in front of the transmitter antenna for phase or amplitude OAM, respectively. Experimental techniques to monitor OAM system involved investigating the received signal power and the number of good data packet received per second.

The layout of this paper is in the following order: section II describes the simulation process and results; section III explains the practical measurements of the proposed system, while the simulated and measured experimental results are illustrated in section IV. Finally, a conclusion to the paper is drawn in section V.

The authors are with the School of Computer Science and Electronic Engineering, University of Essex, Wivenhoe Park, Colchester, CO4 3SQ, Essex, United Kingdom (e-mail: feslam@essex.ac.uk; stuwal@essex.ac.uk).

II. Simulations

Matlab simulation software was exploited for modeling the generation of an OAM state in the 60-GHz wireless channel environment. Prior to performing any simulations, the characteristic of the 60-GHz radiation pattern was measured to be approximately Gaussian and this latter profile was used in the simulations. The OAM states were generated operating both HP and SPP (Fig. 1). During all the simulation processes, it was assumed that HP and SPP were placed directly in front of the 60-GHz transmitter antenna.

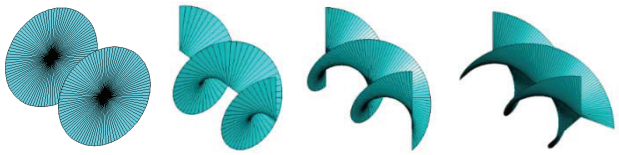

a b c d

Fig. 1 OAM state simulation, (a) L=0 (no OAM), (b) L=1, (c) L=2, (d) L=3.

A. HP

A fork-grating dislocation in a HP (Fig. 2a-c) is the main feature of holographic masks, which creates an OAM state from the plane input wave. The number of phase twists produced around the vortex, in addition to the shape and behavior of fork-grating, are controlled by the topological charge (L) [16]. A holographic interference pattern is the product of the phase-only interference of an indirect plane reference wave which generates a radio vortex beam using the following formula [17, 18]:

$$I(x,y) = \frac{1}{2}\left\{1 + cos\left[L.arctan\left(\frac{y}{x}\right) - 2\pi Kx + \Phi_0\right]\right\} \quad (1)$$

where, (x, y) are the transverse cylindrical coordinates, L is the topological charge of the radio vortex to be created, Φ_0 is an arbitrary phase factor and K is the number of grating lines per unit length.

Simulation of HP masks was applied in a horizontally separated pattern (Fig. 2a-c) with a central dislocation, corresponding to the L value of each mask, as a phase grating which generated OAM state. The outcome of passing the input 60-GHz signal through the disturbance section in the middle of the horizontally (or vertically) separated HP mask is a diffraction-limited beam thus, creating OAM state in the far-field region. Two circular rotating diffraction beam patterns were predicted for the OAM state of input beam, these should appear on both adjacent sides of the middle Gaussian beam for a horizontally separated HP (Fig. 2d-f). Each rotating ring-shaped beam represents the L value of the HP thus, two OAM beam appear, one with positive (e.g. L= +1) having an anti-clockwise rotation and one with negative (e.g. L= -1) value with clockwise rotation on the right and left side of central beam signal, respectively.

The HP behavior was analyzed by simulating and plotting the intensity distribution of the far field diffraction pattern of horizontally separated configuration for L of 1, 3, and 5 (Fig. 9a-c).

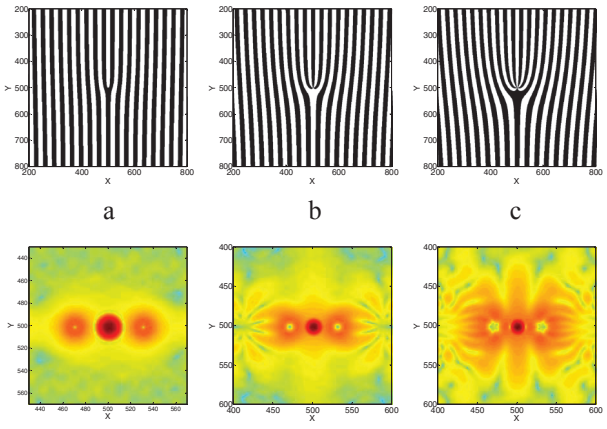

a b c

d e f

Fig. 2 Horizontally separated HP simulations for L= 1, 3, and 5; (a-c) holographic mask, (d-f) corresponding far-field diffraction pattern.

B. *Superimposed HP*

A method of increasing the total number of OAM states from one HP mask is to superimpose two HP masks with, for example, horizontally (L=1) and vertically (L=3) separated format in order to generate a complex HP configuration mask (Fig. 3a). The simulation result for far-field diffraction pattern of mentioned superimposed HP revealed that a total number of 8 OAM states were created in comparison with only two using either of HP masks alone (Fig. 3b-c). Therefore, increasing the complexity of HP masks will generate extra OAM states. The intensity distributions of superimposed far-field diffraction pattern, in Fig. 4, illustrate that the intensity of OAM signal has reduced when compared to using only one HP mask. As a result of the more complex HP pattern, variation in amplitude has further attenuated the signal strength.

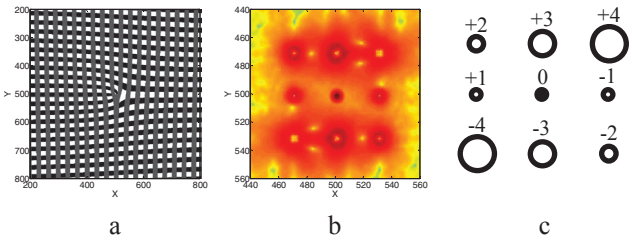

a b c

Fig. 3 (a) HP superimposed mask for L=3 vertically separated and L=1 horizontally separated, (b) corresponding far-field diffraction pattern of 'a', (c) far-field diffraction with OAM representation.

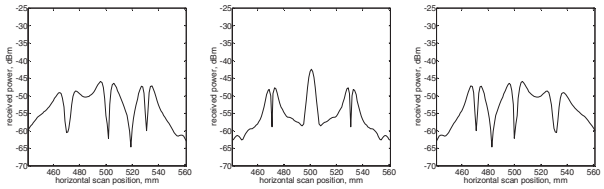

a b c

Fig. 4 Superimposed HP intensity distribution for, (a) lower section, (b) middle section, (c) upper section.

C. *SPP*

Phase alteration of an incoming radio signal is another method for generating OAM state using SPP around 2π phase shift. An infinite number of OAM states are possible theoretically [8, 10, 19], hence the input radio signal power will not be reduced as much as in the HP technique.

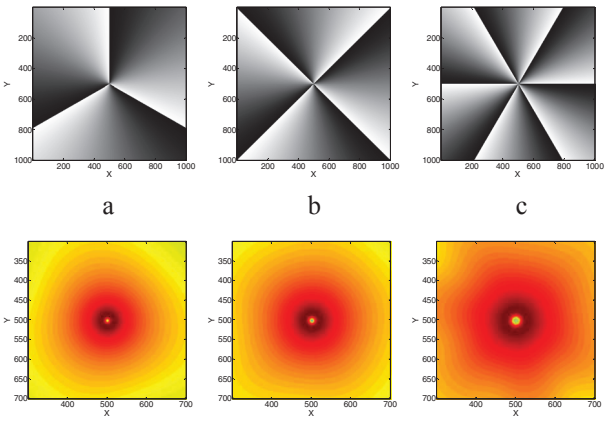

a b c

d e f

Fig. 5 Spiral phase plate simulations for L=3, 4, and 6; (a-c) phase mask simulation, (d-f) corresponding far-field diffraction pattern.

The SPP step height has a direct and linear relationship with the L value (Fig. 8b) and can be calculated with the following formula [20, 21]:

$$L = \frac{\Delta n.h}{\lambda} \quad (2)$$

where, Δn is the difference of refractive index between the SPP and its surrounding (which is usually air), h is the step height of SPP and λ is the wavelength of the incident radio beam, which is 5 mm at 60-GHz. The SPP transmittance is calculated with the following formula [22-26]:

$$f_L(x, y) = exp\ [iL\varphi(x, y)] \quad (3)$$

where, (x, y) are the transverse cylindrical coordinates, L is the topological charge for the phase singularity and φ is the phase of the signal.

The attribute of SPP was examined when a plane Gaussian beam was transmitted through the SPP and an OAM signal detected from the diffracted signal. The simulation of the SPP for L values of 3, 4, and 6 included darker and lighter portions corresponding to -π radian and +π radian, respectively (Fig. 5a-c). Similar to the HP method, OAM signal state were simulated as a diffracted rotating ring-shaped beam in the far-field zone (Fig. 5d-f). The diffraction pattern of OAM signal was investigated in intensity distribution format across the horizontal scan (Fig. 9d-f).

III. Measurements

An OFDM wireless 60-GHz mm-wave reference system (Fig. 6) was utilized to validate the feasibility of OAM radio by transferring a 4-Gbps uncompressed video content. Both the transmitter and receiver antenna are set, by a GUI control interface, to 'lock straight beam' which is useful to concentrate the 60-GHz signal beam. In addition, a brass plate with 5mm gap in the middle was utilized to localize the transmitted signal before it was radiated onto HP or SPP surface. The wavelength at 60-GHz frequency has a direct link with the size of the gap on the brass plate.

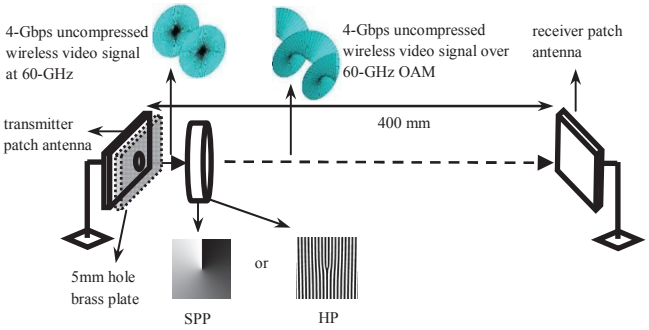

Fig. 6 A 4-Gbps uncompressed wireless OAM experimental setup

As shown in Fig. 7, in order to manufacture the realistic model of HP masks with different L value, the simulation output of Matlab was employed to control a printed circuit board (PCB) router to drill copper plates with required shapes. A realistic prototype of SPP (Fig. 8a) with adjustable step height was manufactured using Polytetrafluoroethylene (PTFE), well known as Teflon. Additionally, the step height was changed to choose different L value.

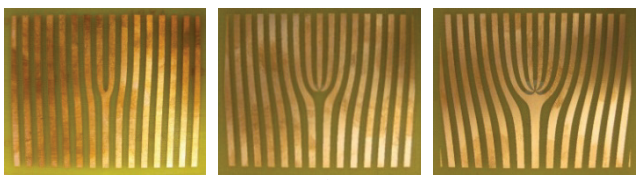

a b c

Fig. 7 HP realistic model, (a) L=1, (b) L=3, (c) L=5

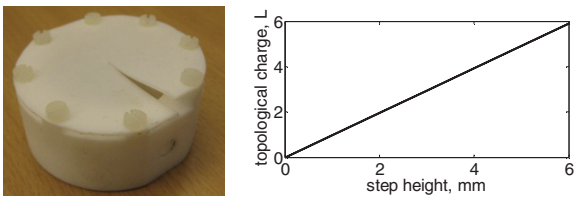

Fig. 8 (a) SPP practical model; (b) Characteristic of SPP as step height is raised

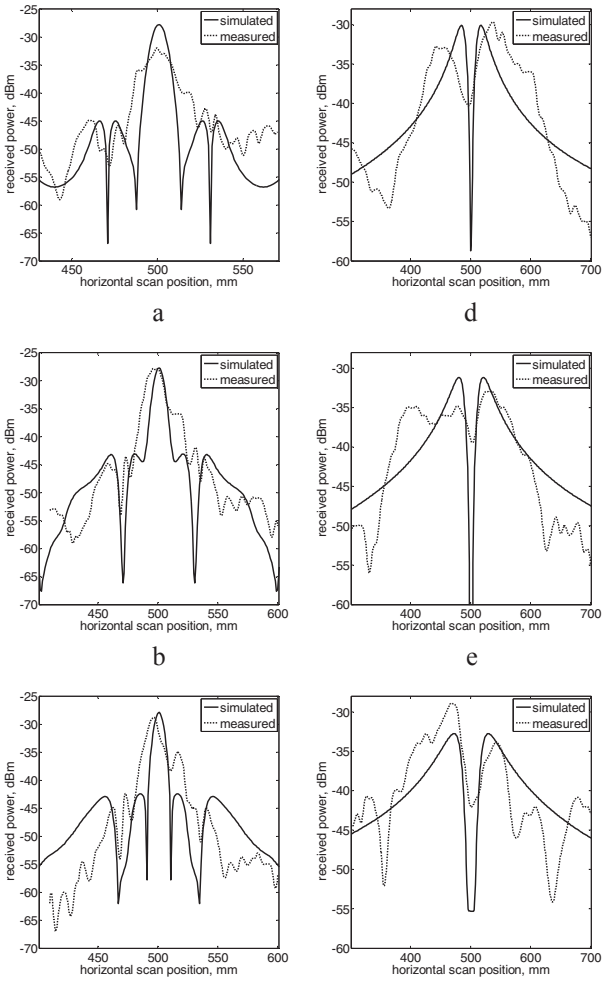

Fig. 9 Measured and simulated intensity distribution of far-field diffraction pattern when utilizing (a-c) HP with L=1, 3, and 5; (d-f) SPP with L=3, 4, and 6.

IV. Results and Discussion

A. Amplitude OAM

The measured intensity distribution results representing the OAM far-field diffraction pattern while utilizing various HP masks is demonstrated in Fig. 9a-c. The signal strength was measured across a horizontal scan for a range of topological charges (L= 1, 3, and 5).

It can be seen from the intensity distribution graph that the Gaussian beam with no OAM state (e.g. L=0) is represented by the middle peak amplitude and OAM states (e.g. L= +1 or L= -1) of the 60-GHz radio beam is signified by other two peak amplitude on either side of the Gaussian beam.

B. Phase OAM

In SPP method, various step height settings were utilized to measure the intensity distribution of the OAM far-field diffraction pattern as it is illustrated in Fig. 9d-f. A range of topological charges (L= 3, 4, and 6) were used to measure the signal strength across a horizontal scan. The existence of OAM in radio domain is observable from the reduced received power strength in the middle of two spikes in the diffraction pattern of signal intensity across a horizontal scan. In addition, the number of good packets per second using SPP method was measured and plotted across the distance of horizontal scan (Fig. 10). The influence of OAM mode is clearly visible on 4-Gbps uncompressed video transmission.

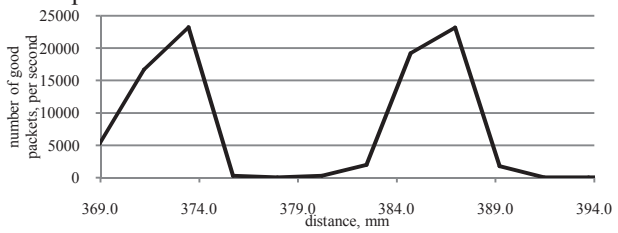

Fig. 10 Measured number of good packets with SPP in use

V. Conclusion

We have described a method of generating OAM state in mm-wave signals by creating HP masks. Matlab simulation was utilized to produce HP masks on a PCB. We believe the experimental measurement demonstrated is the first illustration of 4-Gbps uncompressed video transmission over a 60-GHz OAM wireless channel. It is evident that simulations and experiments are in good agreement. The advantage of utilizing the 60-GHz domain is the narrow beam-width feature, which facilitates OAM generation and spatial multiplexing of separate data. Moreover, the 60-GHz region provides high degree of spectrum reuse for multiple wireless links. Future opportunities for further increase in wireless channel capacity, spatial multiplexing based on OAM and holographic beam-forming are offered as the use of 60-GHz technology becomes more wide spread with the advent of IEEE802.11ad-based modules.

VI. References

[1] S. Q. Xiao, M. T. Zhou, and Y. Zhang, *Millimeter wave technology in wireless PAN, LAN, and MAN*: CRC Press, 2008.

[2] R. C. Daniels and R. W. Heath, "60 GHz wireless communications: emerging requirements and design recommendations," *Vehicular Technology Magazine, IEEE,* vol. 2, pp. 41-50, 2007.

[3] D. Cabric, M. S. W. Chen, D. A. Sobel, Y. Jing, and R. W. Brodersen, "Future wireless systems: UWB, 60GHz, and cognitive radios," in *Custom Integrated Circuits Conference, 2005. Proceedings of the IEEE 2005*, 2005, pp. 793-796.

[4] J. Noreus, M. Flament, and A. Alping, "System considerations for hardware parameters in a 60 GHz WLAN," *Power,* vol. 3, p. 17, 2000.

[5] U. Madhow, "Broadband millimeter wave networks: Architectures and applications," 2008, pp. 1-3.

[6] Z. Hao and T. A. Gulliver, "On the capacity of 60 GHz wireless communications," in *Electrical and Computer Engineering, 2009. CCECE '09. Canadian Conference on*, 2009, pp. 936-939.

[7] A. V. Carpentier, H. Michinel, J. R. Salgueiro, and D. Olivieri, "Making optical vortices with computer-generated holograms," *American Journal of Physics,* vol. 76, pp. 916-921, 2008.

[8] G. Gibson, J. Courtial, M. Padgett, M. Vasnetsov, V. Pas'ko, S. Barnett, and S. Franke-Arnold, "Free-space information transfer using light beams carrying orbital angular momentum," *Opt. Express,* vol. 12, pp. 5448-5456, 2004.

[9] A. M. Yao and M. J. Padgett, "Orbital angular momentum: origins, behavior and applications," *Adv. Opt. Photon.,* vol. 3, pp. 161-204, 2011.

[10] F. Tamburini, E. Mari, A. Sponselli, F. Romanato, B. Thidé, A. Bianchini, L. Palmieri, and C. G. Someda, "Encoding many channels in the same frequency through radio vorticity: first experimental test," *Arxiv preprint arXiv:1107.2348,* 2011.

[11] F. Tamburini, E. Mari, B. Thidé, C. Barbieri, and F. Romanato, "Experimental verification of photon angular momentum and vorticity with radio techniques," *Applied Physics Letters,* vol. 99, pp. 204102-204102-3, 2011.

[12] F. Tamburini, B. Thide, G. Molina-Terriza, and G. Anzolin, "Twisting of light around rotating black holes," *Nat Phys,* vol. 7, pp. 195-197, 2011.

[13] B. Thidé, F. Tamburini, E. Mari, F. Romanato, and C. Barbieri, "Radio beam vorticity and orbital angular momentum," *Arxiv preprint arXiv:1101.6015,* 2011.

[14] S. M. Mohammadi, L. K. S. Daldorff, J. E. S. Bergman, R. L. Karlsson, B. Thide, K. Forozesh, T. D. Carozzi, and B. Isham, "Orbital Angular Momentum in Radio — A System Study," *Antennas and Propagation, IEEE Transactions on,* vol. 58, pp. 565-572, 2010.

[15] (2012). *Silicon Image - Enhancing the connected HD experience*. Available: http://www.siliconimage.com

[16] J. P. Torres and L. Torner, *Twisted Photons: Applications of Light with Orbital Angular Momentum*: Wiley-VCH, 2011.

[17] J. Strohaber, T. D. Scarborough, and C. J. G. J. Uiterwaal, "Ultrashort intense-field optical vortices produced with laser-etched mirrors," *Appl. Opt.,* vol. 46, pp. 8583-8590, 2007.

[18] J. Arlt, K. Dholakia, L. Allen, and M. Padgett, "The production of multiringed Laguerre–Gaussian modes by computer-generated holograms," *Journal of Modern Optics,* vol. 45, pp. 1231-1237, 1998.

[19] J. B. Götte, K. O'Holleran, D. Preece, F. Flossmann, S. Franke-Arnold, S. M. Barnett, and M. J. Padgett, "Light beams with fractional orbital angular momentum and their vortex structure," *Opt. Express,* vol. 16, pp. 993-1006, 2008.

[20] S. S. R. Oemrawsingh, J. A. W. van Houwelingen, E. R. Eliel, J. P. Woerdman, E. J. K. Verstegen, J. G. Kloosterboer, and G. W. t Hooft, "Production and Characterization of Spiral Phase Plates for Optical Wavelengths," *Appl. Opt.,* vol. 43, pp. 688-694, 2004.

[21] M. Soskin, V. Gorshkov, M. Vasnetsov, J. Malos, and N. Heckenberg, "Topological charge and angular momentum of light beams carrying optical vortices," *Physical Review A,* vol. 56, p. 4064, 1997.

[22] V. V. Kotlyar, A. A. Almazov, S. N. Khonina, V. A. Soifer, H. Elfstrom, and J. Turunen, "Generation of phase singularity through diffracting a plane or Gaussian beam by a spiral phase plate," *J. Opt. Soc. Am. A,* vol. 22, pp. 849-861, 2005.

[23] L. Allen, M. W. Beijersbergen, R. J. C. Spreeuw, and J. P. Woerdman, "Orbital angular momentum of light and the transformation of laguerre-gaussian laser modes," *Phys. Rev. A,* vol. 45, pp. 8185-8189, 1992.

[24] Q. Wang, X. W. Sun, and P. Shum, "Generating Doughnut-Shaped Beams with Large Charge Numbers by Use of Liquid-Crystal Spiral Phase Plates," *Appl. Opt.,* vol. 43, pp. 2292-2297, 2004.

[25] C. Jun, K. Deng-Feng, G. Min, and F. Zhi-Liang, "Generation of optical vortex using a spiral phase plate fabricated in quartz by direct laser writing and inductively coupled plasma etching," *Chinese Physics Letters,* vol. 26, p. 014202, 2009.

[26] C. Rotschild, S. Zommer, S. Moed, O. Hershcovitz, and S. G. Lipson, "Adjustable Spiral Phase Plate," *Appl. Opt.,* vol. 43, pp. 2397-2399, 2004.